Crystal structure of the phosphatidylethanolamine-binding protein from bovine brain: a novel structural class of phospholipid-binding proteins

Laurence Serre*, Béatrice Vallée, Nicole Bureaud, Françoise Schoentgen and Charles Zelwer

Background: Phosphatidylethanolamine-binding protein (PEBP) is a basic protein found in numerous tissues from a wide range of species. The screening of gene and protein data banks defines a family of PEBP-related proteins that are present in a variety of organisms, including *Drosophila* and inferior eukaryotes. PEBP binds to phosphatidylethanolamine and nucleotides *in vitro*, but its biological function *in vivo* is not yet known. The expression of PEBP and related proteins seems to be correlated with development and cell morphogenesis, however. To obtain new insights into the PEBP family and its potential functions, we initiated a crystallographic study of bovine brain PEPB.

Results: The X-ray crystal structure of bovine brain PEBP has been solved using multiple isomorphous replacement methods, and refined to 1.84 Å resolution. The structure displays a β fold and exhibits one nonprolyl *cis* peptide bond. Analysis of cavities within the structure and sequence alignments were used to identify a putative ligand-binding site. This binding site is defined by residues of the C-terminal helix and the residues His85, Asp69, Gly109 and Tyr119. This site also corresponds to the binding site of phosphorylethanolamine, the polar head group of phosphatidylethanolamine.

Conclusions: This study shows that PEBP is not related to the G-protein family nor to known lipid-binding proteins, and therefore defines a novel structural family of phospholipid-binding proteins. The PEBP structure contains no internal hydrophobic pocket, as described for lipocalins or small phospholipid-transfer proteins. Nevertheless, in PEBP, a small cavity close to the protein surface has a high affinity for anions, such as phosphate and acetate, and also phosphorylethanolamine. We suggest that this cavity corresponds to the binding site of the polar head group of phosphatidylethanolamine.

Address: Centre de Biophysique Moléculaire, Centre National de la Recherche Scientifique, UPR 4301, affiliated to the University of Orléans, rue Charles Sadron, 45071 Orléans Cedex 2, France.

*Corresponding author.
E-mail: laurence@cnrs-orleans.fr

Key words: *cis* peptide, crystal, Greek key, phospholipid, protein

Received: **6 July 1998**
Revisions requested: **5 August 1998**
Revisions received: **17 August 1998**
Accepted: **18 August 1998**

Structure 15 October 1998, **6**:1255–1265
http://biomednet.com/elecref/0969212600601255

Introduction

In 1984, Bernier and Jollès purified a soluble basic protein with a significant affinity for organic anions from bovine brain [1]. As affinity experiments showed that this protein could interact *in vitro* with phosphatidylethanolamine, a component of cell membranes, it was called phosphatidylethanolamine-binding protein (PEBP) [2]. In addition, it was demonstrated that the bovine PEBP could bind mononucleotides and dinucleotides (mainly GTP) *in vitro* [3]. Homologous PEBPs were subsequently identified in numerous tissues from mammalian species [4]: human (liver [5] and brain [6,7]), monkey (epididymis and testis [8]) and rat (brain [9], epididymis and testis [8]). PEBP was characterized as a single polypeptide chain of 186 or 187 amino acids with a molecular weight of about 21 kDa [10]. Comparisons with other primary sequences did not reveal any significant identity with proteins of known three-dimensional structure, suggesting that PEBP might represent a novel protein family [10]. More recently, the screening of gene and protein data banks identified a family of proteins related to PEBP. Members of this family include a potential odorant-binding protein (OBP) found in the antenna of *Drosophila* [11], Ag16, an antigen recognized by immune sera from patients infected by the parasite *Onchocerca volvulus* [12], TES-26, a secreted antigen of infective larvae of the ascaride nematode parasite *Toxocara canis* [13], TFS1, a suppressor of *CDC25* mutations in *Saccharomyces cerevisiae* [14], *Antirrhinum* CEN, a protein involved in inflorescence development [15] and a putative PEBP from *Plasmodium falciparum* [16]. Thus, the PEBP-related proteins seem to constitute a new widespread protein family. Apart from the affinity of mammalian PEBPs for nucleotides and phospholipids, little information is available concerning

the accurate physiological function of the PEBP family; however, it seems to be correlated with tissue development and cellular morphogenesis. Indeed, PEBP is encountered in oligodendrocytes of developing rat brains and in elongated spermatides during rat spermatogenesis [8,9]. Similarly, TFS1 seems to be involved in yeast growth [14], and recessive mutations in the CEN gene result in the conversion of the normal indeterminate inflorescence to a determinate inflorescence in *Antirrhinum* [15]. Until now, however, no structural experimental data were available for this protein family, apart from a predicted model of PEBP based on weak primary and secondary structure similarities between bovine brain PEBP and the N-terminal domain of yeast phosphoglycerate kinase [17]. This work suggested that PEBP had a potential nucleotide-binding site with a Rossmann-fold topology [18]. To obtain new insights into the PEBP family and its potential functions, we initiated a crystallographic study of bovine brain PEBP.

In this paper, we report the first crystal structure of a member of the PEBP family at 1.8 Å resolution. This work shows that bovine brain PEBP constitutes a novel class of phospholipid-binding protein. In addition, the X-ray structure of a PEBP–phosphorylethanolamine complex at 2.25 Å resolution is presented, allowing a putative phospholipid-binding site to be defined. The binding of GTP and the hypothetical biological function of PEBP are also discussed.

Results

Bovine brain PEBP was crystallized in both monoclinic and orthorhombic forms. The Cα atom superimposition of both crystal form models led to low root mean square (rms) deviations (0.438 Å and 0.506 Å for each monomer, given by the LSQ option of the program O [19]), indicating no major differences between the two structures. In light of this, and because the structure solved from the monoclinic crystal was refined to a higher resolution, we will focus mainly on the monoclinic crystal structure.

Quality of the atomic model

The final atomic model consists of 1466 nonhydrogen atoms, 247 water molecules and one well-ordered molecule of acetate buffer (reported as ACT in the PDB coordinates file). The PEBP model includes residues 1–185 of the polypeptide chain; the C-terminal Lys186 is the only residue not defined by the electron-density map. The stereochemistry of the model was checked with PROCHECK [20] and shows no disagreement with the general stereochemistry rules. Of the total number of residues, 92.7% are found in the most favored regions of the Ramachandran plot and 7.3% in the additional allowed regions. The structure reveals two *cis* peptide bonds: between Ala72 and Pro73, and between Arg81 and Glu82. Observed rms deviations from ideal values of bond lengths and bond angles are 0.011 Å and 2.182°, respectively. The overall coordinate error is estimated between 0.12 and 0.15 Å from a Luzzati plot. The mean atomic temperature factor for the whole model is 12.0 Å^2, including solvent molecules.

General fold

The PEBP structure is made up of one unique domain and has a β fold (Figure 1). This domain is formed by two antiparallel β sheets having a Greek-key topology, and a C-terminal αβα element. Both β sheets interact with each other through a hydrophobic interface. The structure is also characterized by long loops connecting the different secondary structure elements. The PEBP model is rich in β-turn structures and exhibits three short 3_{10} helical regions (residues 5–7, 13–15 and 96–99). PEBP secondary structures were assessed according to DSSP convention [21] (see Figure 1 legend). Comparison with known protein structures (using the program DALI [22]) did not reveal any folds from other protein structures that would superimpose well. The best score was 4.3 for the Rho GDP-dissociation inhibitor (RhoGDI; PDB code 1gdh) which has a distinct β fold [23].

The *cis* peptide bonds

Both *cis* peptide bonds of PEPB are located after a β turn (residues 69–72) in the loop connecting β strand S5 to β strand S6. The *cis* Pro73 is located at the top of the loop interacting with the sidechain atom Nε2 of His117 (Figure 2a). The nonprolyl *cis* peptide bond, between Arg81 and Glu82, occurs between a β turn (residues 78–81) and the N-terminal extremity of β strand S6 (Figure 2a). Because of this configuration, two Cα atoms of Arg81 and Glu82 are positioned within 3.0 Å of each other (Figure 2b). Figure 2c also shows that the peptide bond between Arg81 and Glu82 is not planar; this is due to the backbone amide group of Glu82, which is 0.19 Å above the plane defined by the peptide bond atoms. Arg81 and Glu82 are well stabilized in the structure. The *cis* peptide bond atoms can form two hydrogen bonds: one with the mainchain carbonyl of Phe148 (hydrogen-bond distance N_{Glu82}–O_{Phe148}, 2.78 Å) and one with the sidechain amine group of Lys147 (hydrogen-bond distance O_{Glu82}–$N\zeta_{Lys147}$, 2.86 Å) (Figure 2a). The sidechains of Arg81 and Glu82 are also stabilized by numerous hydrogen bonds with neighboring residues (Figure 2a). Another unusual feature is the close contacts of the Cβ atom of Glu82 with the mainchain carbonyl of Phe148 (distance 3.05 Å) and with the sidechain Oγ1 atom of Thr68 (distance 3.14 Å), which contributes to constrain the Glu82 conformation. The omit map calculated around this *cis* peptide bond is shown in Figure 2d.

The ligand-binding site

An accessibility calculation using the program VOIDOO [24] shows that the PEBP structure is rather compact. A

Figure 1

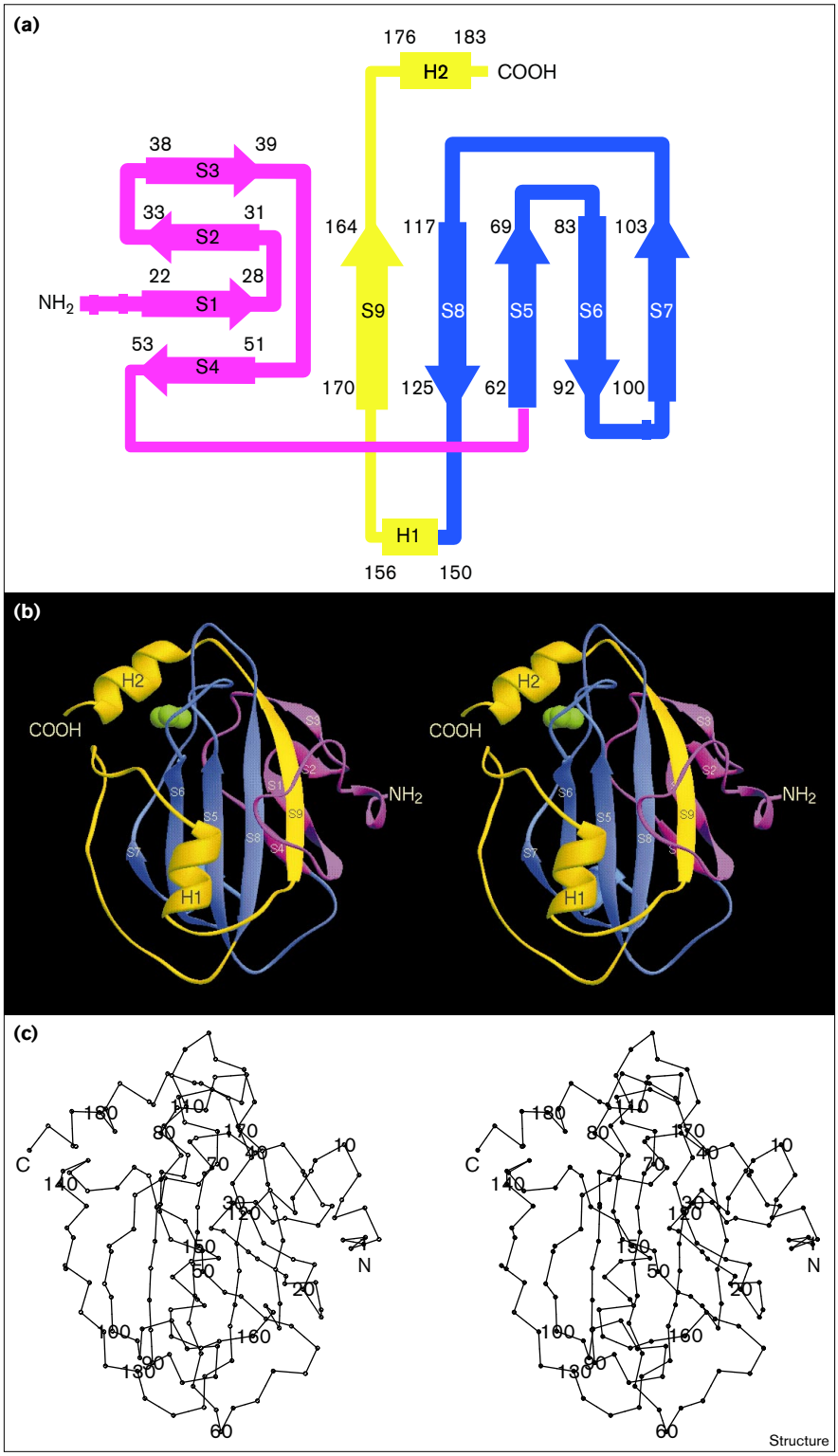

The general architecture of bovine brain PEBP. **(a)** A topology diagram of PEBP; β strands are symbolized by arrows and α helices by rectangles. Residues with 3_{10} helicity are represented by bars. β Sheet 1 (in magenta) is formed by four antiparallel strands: S1 (residues 22–28), S2 (residues 31–33), S3 (residues 38–39) and S4 (residues 51–53). β Sheet 2 (in purple) is also formed by four antiparallel strands: S5 (residues 62–69), S6 (residues 83–92), S7 (residues 100–103) and S8 (residues 117–125). β Sheet 2 is terminated by an αβα extension (yellow) comprising helix H1 (residues 150–156), strand S9 (residues 164–170) and helix H2 (residues 176–183). **(b)** Stereoview ribbon model of PEBP. The bound acetate molecule is represented by green spheres. Both Greek-key motifs are colored in magenta and purple, as in (a); the αβα unit is indicated in yellow. **(c)** Stereoview Cα backbone trace of PEBP, every tenth residue is labeled and the N and C termini are indicated. (The figures were generated using the programs RIBBONS, version 2.80 [50] and MOLSCRIPT [51].)

single cavity was detected; this cavity is narrow and located close to the protein surface (Figure 3). The cavity is formed by residues of the C-terminal helix (Leu179, Tyr180 and Leu183) and two strand-connecting regions of β sheet 2 (Asp69, Ala72, Trp83, His85, Val106, Gly109, Pro110, Pro111, His117 and Tyr119; Figure 4). The

Figure 2

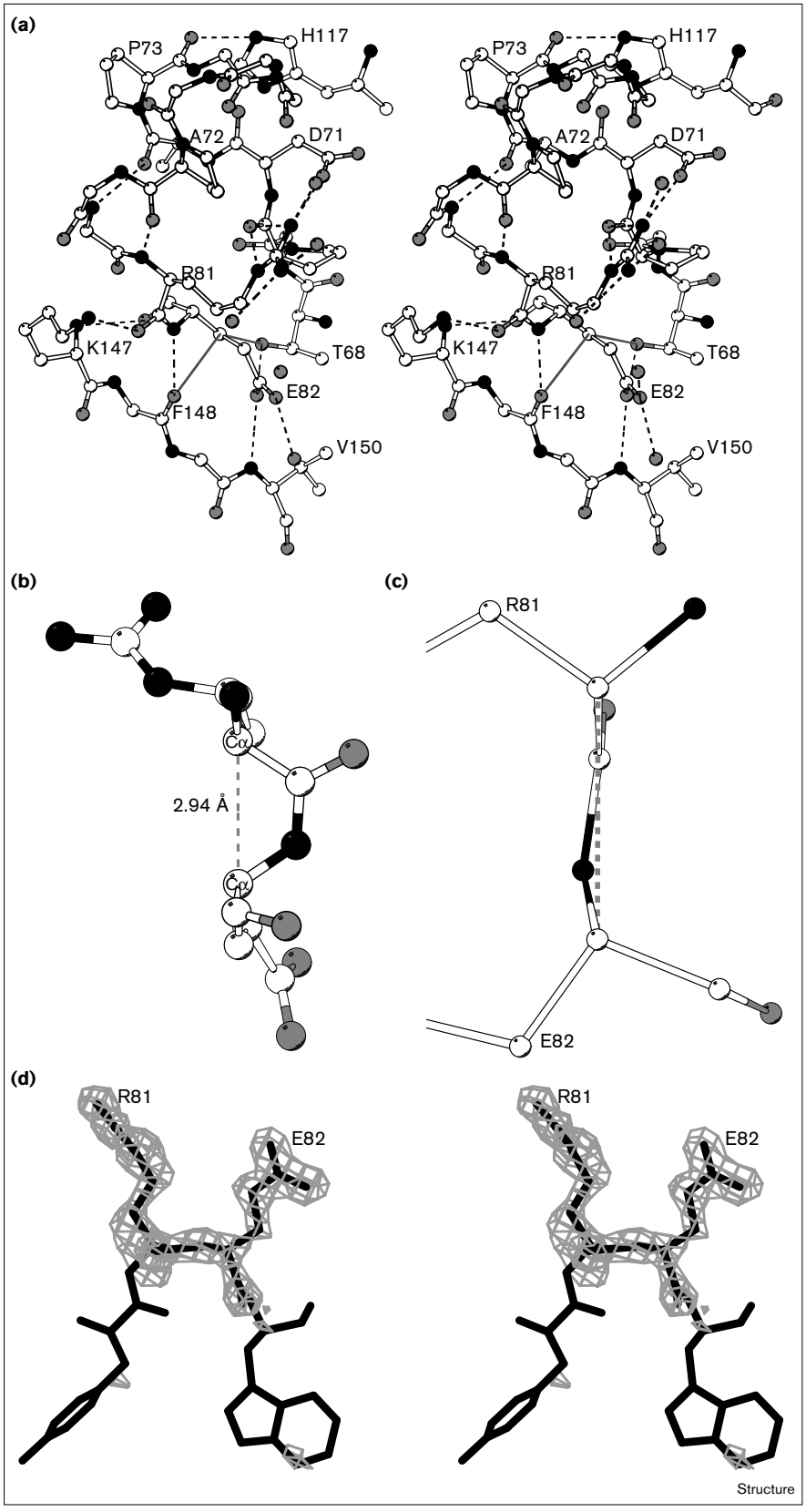

The nonprolyl *cis* peptide bond between Arg81 and Glu82. **(a)** The hydrogen-bond network around the nonprolyl *cis* peptide bond. The short contacts between the Cβ atom of Glu82 and the O atom of Phe148 or Oγ1 of Thr68 are represented by solid lines. Other hydrogen bonds are shown as dashed lines. Carbon atoms are shown in white, nitrogen atoms in black and oxygen atoms in gray. For clarity, some sidechains were omitted. **(b)** The short contact between the Cα atoms of Arg81 and Glu82. **(c)** The nonprolyl *cis* peptide bond is nonplanar; the peptide bond plane is symbolized by a dashed line. **(d)** The omit map around residues 81–85. The map was calculated with the coefficients ($mF_{obs}–DF_{calc}$) [52] between 32 and 1.84 Å resolution, after Arg81 and Glu82 were removed from the coordinate model and a simulated-annealing cycle was carried out at 3000K. The electron-density map is contoured at a 3σ level. (The figures were generated using the program MOLSCRIPT [51] and the electron-density was created with the program O [19].)

Figure 3

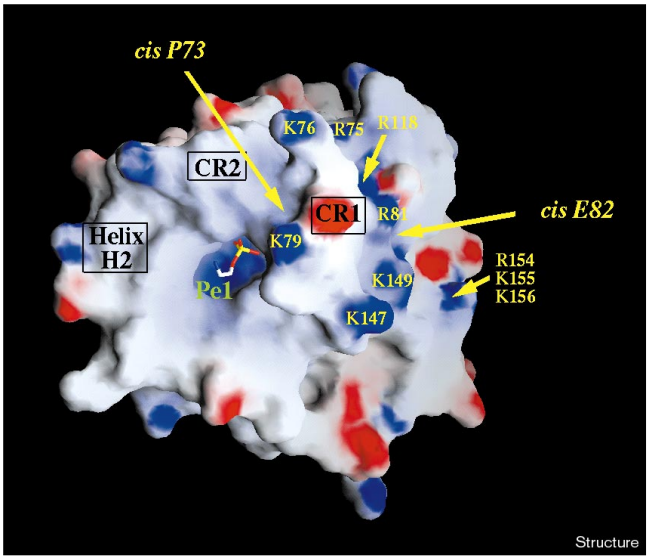

The electrostatic surface potential of PEBP. The bound phosphorylethanolamine is shown in the cavity in ball-and-stick representation. Regions of negative potential are shown in red; regions of positive potential are in blue. The strip of basic residues is labeled in yellow. CR1 and CR2 represent strand-connecting regions 1 and 2, respectively. (The figure was created using the program GRASP [25].)

strand-connecting regions are defined as CR1 (residues 68–85) and CR2 (residues 106–119). Electrostatic potential surface analysis using GRASP [25] highlights a strip of basic residues close to this cavity (Arg75, Lys76, Lys79, Arg81, Arg118, Lys147, Lys149, Arg154, Lys155 and Lys156; Figure 3). Among these basic residues, Arg118 is conserved among the different members of the PEBP family and is involved in the formation of a salt bridge with Asp71, another conserved residue. Both *cis* peptide bonds of the structure are found in close proximity to this cavity (Figures 3 and 4). In the three different crystal structures obtained — in the presence of phosphate, acetate or phosphorylethanolamine — an anion group occupies this site. In the monoclinic crystals, we modeled a molecule of acetate hydrogen bonded to the amide group of Gly109 (hydrogen-bond distance 2.76 Å), to the Nε2 of His85 (hydrogen-bond distance 2.98 Å) and to water molecules (Figures 4 and 5a). The methyl group of the acetate molecule is surrounded by hydrophobic residues (Trp83, Val106, Tyr180 and Leu183). In the orthorhombic crystals, the Fourier difference $(mF_{obs}–DF_{calc})\exp(\phi_{calc})$ map calculated after a first refinement cycle, for data between 15 and 2.4 Å, exhibits a high peak in this putative binding site. The tetrahedral shape of this residual density is compatible with the binding of a phosphate group in the cavity. Modeling indicates that this phosphate ion establishes hydrogen bonds with the sidechains of residues Tyr119, His85, Asp69 and the backbone amide group of Gly109 (Figure 5b). Superimposition of the orthorhombic and monoclinic models shows that the acetate- and phosphate-binding sites overlap (Figures 4 and 5a,b). In addition, these anions superimpose well with the phosphorylethanolamine molecule in the structure of the PEBP–phosphorylethanolamine complex. Phosphorylethanolamine constitutes the polar head group of phosphatidylethanolamine and binds PEBP in two possible ways (indicated as Pe1 and Pe2 in Figures 5c and 5d). The major interaction, Pe1, shows that the phospholipid polar head group establishes hydrogen bonds with His85, Asp69, Gly109 and Tyr119, as described for the phosphate ion. Additional interactions occur between the carbonyl group of Gly109 and the amine group of phosphorylethanolamine, and between the ligand ethyl group and Trp83. The minor interaction, Pe2, involves hydrogen bonds with the phosphate group only.

Discussion

Affinity experiments have shown that PEBP is able to bind phospholipids as well as GTP [3]. Nevertheless, the bovine PEBP structure is neither related to the G protein family [26] nor to known lipid-binding proteins [27–29]. PEPB has a β fold formed by two Greek-key motifs, a motif

Figure 4

The putative ligand-binding site. The carboxylate and methyl groups of the bound acetate molecule are represented in red and green, respectively; the phosphate molecule is colored in purple. Water molecules are represented as small light green spheres and the C-terminal α helix is depicted as a yellow ribbon. The position of the phosphate group was calculated after superimposition of the monoclinic and orthorhombic coordinate models using the LSQ option in the program O [19]. (The figure was generated using the program RIBBONS, version 2.80 [52].)

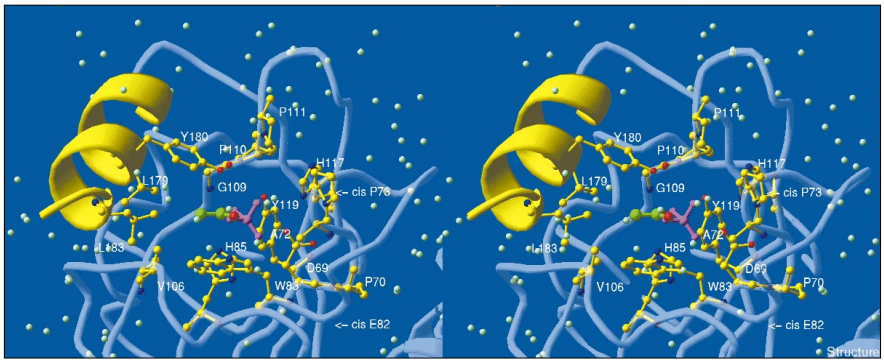

Figure 5

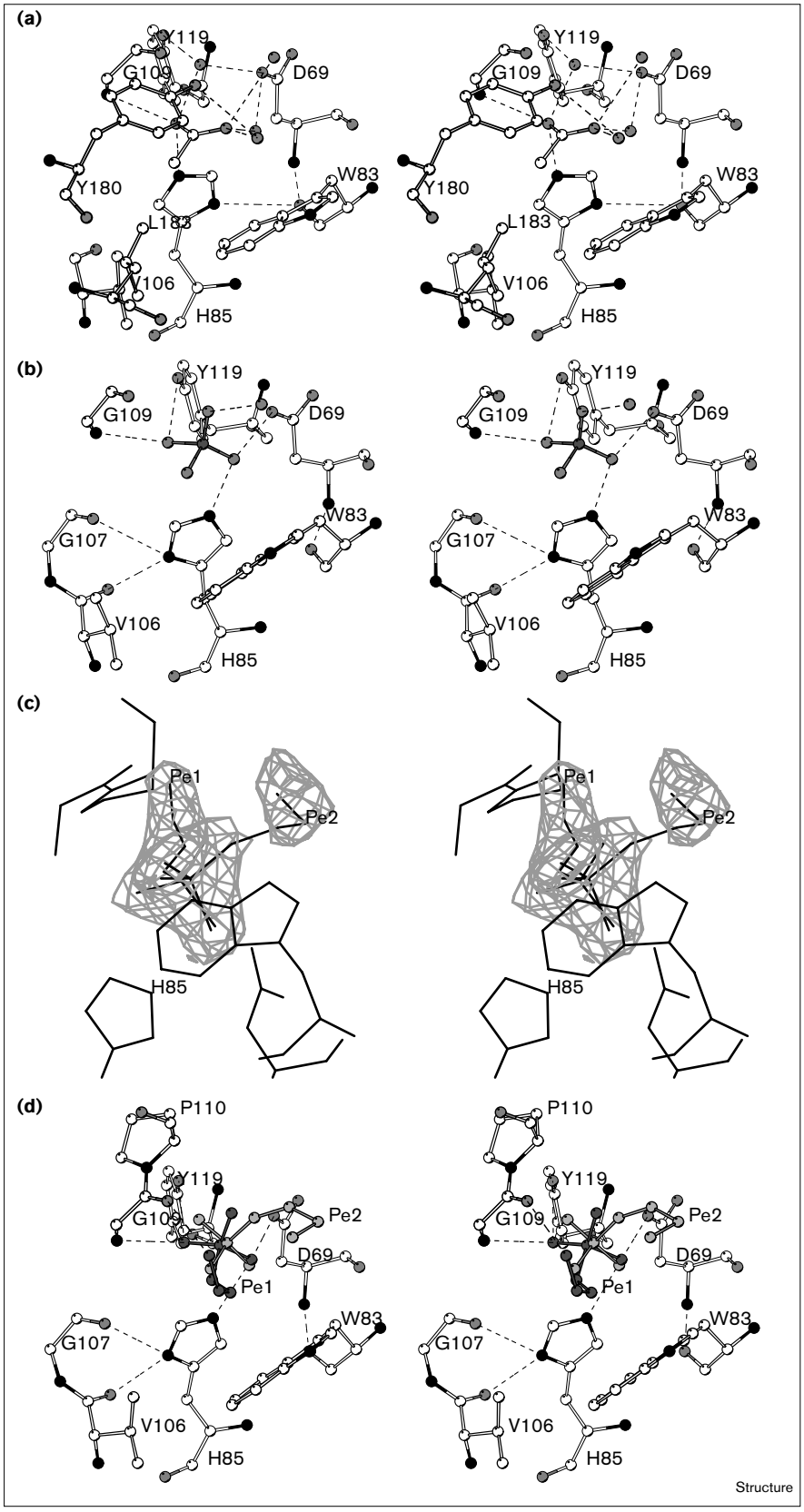

The binding of PEBP to anion groups. **(a)** Stereoview depicting the binding of the acetate molecule. Carbon atoms are shown in white, nitrogen atoms in black and oxygen atoms in gray; hydrogen bonds are shown as dashed lines. **(b)** Stereoview of the phosphate binding. In order to optimize hydrogen bonding, the sidechain of His85 was flipped from its position in the acetate-bound model. **(c)** Stereoview electron-density map calculated around the phosphorylethanolamine molecule ($3mF_o-2DF_c$) with data between 15 and 2.25 Å. The map is contoured at the 1σ level. The two alternative phosphorylethanolamine-binding modes are labeled Pe1 and Pe2. **(d)** Stereoview to illustrate phosphorylethanolamine binding. (The figures were generated using the program MOLSCRIPT [51] and the electron-density was created with the program O [19].)

frequently described for immunoglobin superfamilies. The PEBP structure reported here constitutes the first structure of a novel class of proteins that can interact with both phospholipids and GTP.

The ligand-binding site

The PEBP structure does not contain any internal hydrophobic cavity, as described for Sec14 (a phosphatidylinositol-transfer protein from *Saccharomyces cerevisiae* [27]), lipocalins [28] or small lipid-transfer proteins from plants [29]. However, a small cavity close to the protein surface, involving residues of the C-terminal helix and two strand-connecting regions (CR1 and CR2) of the second Greek key, seems to form the ligand-binding site of PEBP. The volume of this putative ligand-binding site is rather small and we speculate that, if it corresponds to the phospholipid-binding site, only the polar head group of the phospholipid would be recognized. This is in agreement with the binding of a phosphorylethanolamine molecule in the PEBP–phosphorylethanolamine crystal structure.

The CR1 and CR2 regions are comprised of residues that are conserved throughout the PEBP protein family (Figure 6). Among these residues, six are invariant in all the sequences (Pro70, Asp71, Pro73, His85, Gly115 and Arg118). The variant residues could modulate the size and shape of the binding site and induce different ligand specificities for each of these proteins. This concerns mainly residues at positions 72, 80, 83 and 119, which face the binding site (Figure 4).

The CR1 region exhibits two *cis* peptide bonds, between Ala72 and Pro73 and between Arg81 and Glu82, at the boundaries of the ligand-binding site. Nonprolyl *cis* peptide bonds are very rare in protein structures. In 1990, only 0.05% of all peptide bonds listed in the Brookhaven Protein Data Bank (PDB) [30] had a *cis* conformation and, in general, they were located in regions concerned with protein function [31]. In *Vibrio harveiy* luciferase, for example, the nonprolyl *cis* peptide bond occurs in a bulge and is responsible for creating a small cavity at the active site [32]. Moreover, in the PEBP structure, the residues Arg81 and Glu82 are located close to a strip of basic residues that are conserved in all mammalian PEBPs (Figure 3). These basic residues could interact through electrostatic contacts with the negatively charged surface of the membrane layer, as suggested for the calcium/phospholipid-binding C2 domain of cytosolic phospholipase A2 (cPLA2) [33]. Thus, the nonprolyl *cis* peptide bond of PEBP would be located in an area of the protein concerned with membrane binding. Another line of evidence for this region of PEBP having a functional role is provided by the existence of *Arabidopsis* natural mutant plants [34], which develop a single terminal flower instead of the normal indeterminate inflorescence. These *Arabidopsis* mutants are affected in their CEN homologous gene (CEN belongs to the PEBP-related protein family) and the deduced amino acid sequence of one of these natural mutants contains the mutation Glu82→Lys.

On the issue of GTP binding, a model of PEBP predicted on the basis of an alignment with phosphoglycerate kinase, suggested that the consensus sequence of residues 112–125 formed an α/β nucleotide-binding site with Rossmann-fold topology [17]. In our crystal structure, residues 112–125 are indeed found close to the putative ligand-binding site, but they do not belong to a Rossmann fold. Residues 112–125 include β strand S8 and a part of the CR2 region. However, the presence of a phosphate (or a sulfate) ion is often a hallmark for a nucleotide-binding site (e.g. the RNA-binding site of ribonuclease [35] or the $NADP^+$-binding site of ferredoxin $NADP^+$ reductase [36]). Nevertheless, if this cavity does correspond to the GTP-binding site, it seems too narrow to accommodate a whole nucleotide molecule in the absence of any conformational changes. GTP might be recognized by its pyrophosphate group, which could fit into the cavity and would be stabilized by hydrogen bonds with residues His85, Asp69, His117, Gly109 and Tyr119. The GTP pyrophosphate group might also be recognized by the strip of basic residues through electrostatic interactions.

Hypothetical function

Comparison of the PEBP structure with other folds in the PDB gives the highest score for the C-terminal domain of a Rho GDP-dissociation inhibitor (RhoGDI), a protein that negatively regulates Rho family GTPases [23]. This protein has an immunoglobulin-like fold with a modified Greek key β-strand topology. Indeed, the superimposition of the β sheets of this structure and of PEBP is possible, but the strand connectivity is different. In RhoGDI, the two Greek keys are formed by noncontiguous segments in the protein primary sequence. The same observation is made with the Greek-key topology identified in the calcium/phospholipid-binding domain of synaptotagmin I [37], a synaptic vesicle membrane protein, and some phospholipases (cPLA2 [33] and PLCδ1 [38]). The calcium/phospholipid-binding site of these proteins is formed by loops that resemble the PEBP CR1 and CR2 regions. Thus, PEBP could have a similar function and may also be a membrane-binding protein, interacting with other proteins and possibly modulating their catalytic activities. Recently, it was reported that TSF1, a PEBP-related protein, is a carboxypeptidase Y inhibitor, establishing that members of the PEBP family can interact with other proteins [39].

In conclusion, our crystallographic study shows that PEBP is neither related to the G protein family nor to

Figure 6

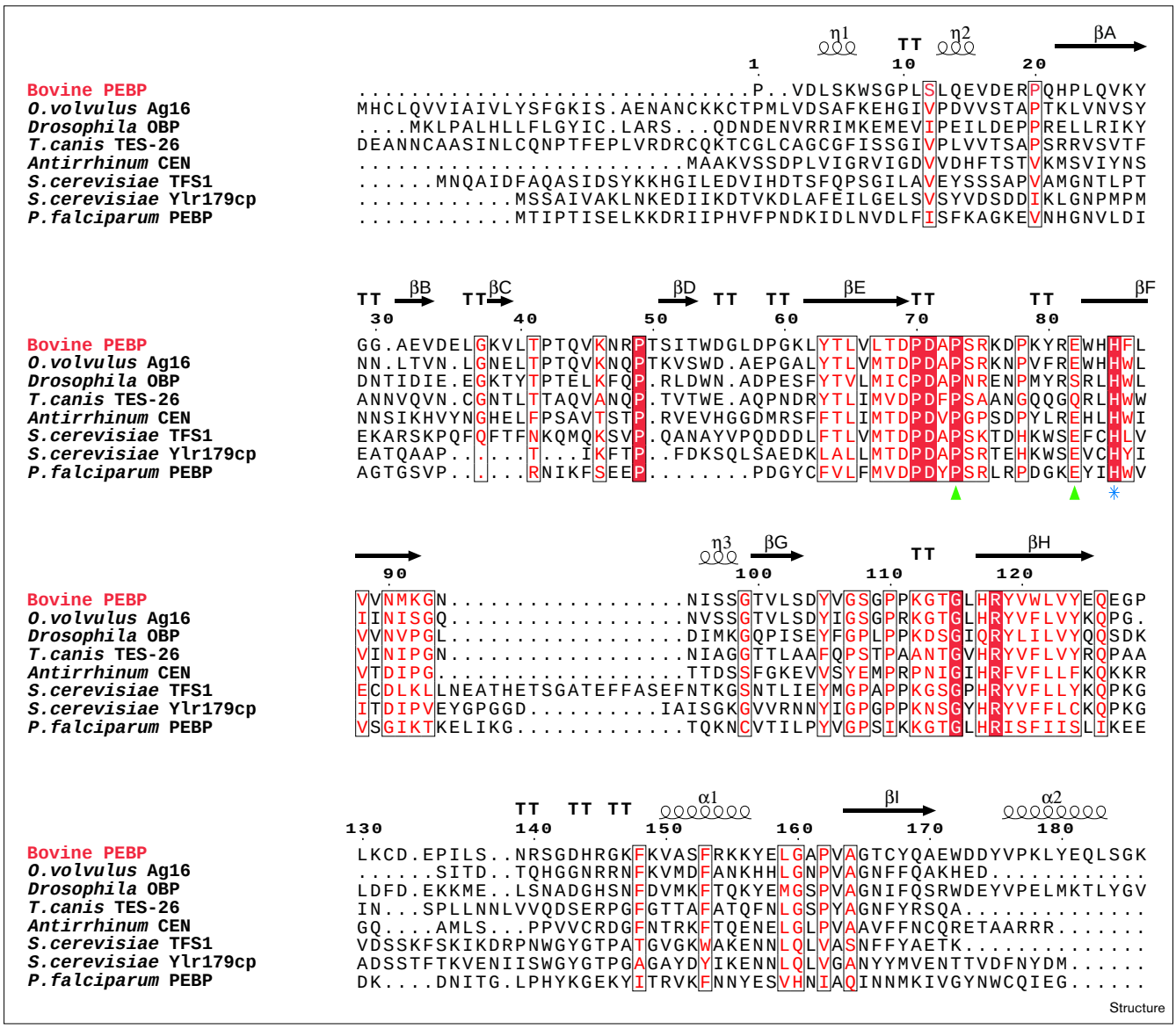

Sequence alignments. The figure shows an alignment of the amino acid sequences of seven members of the PEBP family: bovine brain PEBP [10], *Onchocerca volvulus* Ag16 [12], *Drosophila* OBP [11], *Toxocara canis* TES-26 [13], *Antirrhinum* CEN [15], *Saccharomyces cerevisiae* TFS1 [14], the *ylr179c* gene product of *S. cerevisiae* [53] and *Plasmodium falciparum* PEBP [16]. Sequence homologies are highlighted in red; sequence identities are shown as white letters on a red background. Both of the *cis* peptide bonds are marked by green triangles and His85 is indicated by a blue star. The secondary structure elements of bovine brain PEBP have been added to the figure (assigned according to DSSP): helices are displayed as squiggles and β strands as arrows. TT is used to mark a β turn and η1, η2 and η3 indicate the 3_{10} helices. (The figure was created using ESPrit [P Gouet and F Metoz, unpublished program]).

known lipid-binding proteins, and that its structure defines a novel family of phospholipid-binding proteins. We identify a putative phospholipid-binding site, the role of which has yet to be confirmed by biochemical and mutagenesis experiments. Such experiments will be conducted in parallel with further crystallographic studies to determine the structures of PEBP in complex with GTP and a complete phospholipid molecule. However, understanding the *in vivo* function of this protein and its related family, will require further investigations at the cellular level. For this purpose, the study of mutants, designed with the help of our structure, might help to isolate phenotypes linked to PEBP mutations and will shed some light on the biological function of the PEBP family members and their potential partners in the cell.

Biological implications

Phosphatidylethanolamine-binding protein (PEBP) is a 21 kDa basic protein that was first isolated from bovine brain [1]. It was shown that, *in vitro*, PEBP binds to both phosphatidylethanolamine and GTP [2,3]. Although its precise biological role is still unknown, PEBP has been detected in numerous mammalian tissues, including brain cells, elongated spermatides from testis, placenta and liver [5–9]. Thus, it seems that PEBP is present in cells exhibiting morphogenesis activity. In addition, sequence alignments have shown that mammalian PEBP belongs to a larger family of proteins that seem to be related to developmental processes. Members of this family include CEN [15] (a protein involved in inflorescence architecture control), antigens secreted by parasite larvae [13] and TFS1, a suppressor of *CDC25* mutation in yeast [14].

In order to obtain new insights into PEBP function, we have solved the X-ray crystal structures of bovine brain PEBP both on its own and in complex with phosphorylethanolamine (the polar head group of phosphatitylethanolamine). These structures show that PEBP and PEBP-related proteins constitute a structural protein family that is unrelated to any G-protein family members or to any lipid-binding proteins of known structure. In addition, we have identified the putative phospholipid-binding site of PEBP: a small cavity located close to the protein surface and defined by the residues His85, Asp69, Gly109 and Tyr119.

Although these structures do not yet indicate the precise *in vivo* function of PEBP, they do show that PEBP exhibits some similarities to other proteins: the C-terminal domain of a Rho GDP-dissociation inhibitor, which negatively regulates Rho family GTPases [23]; the calcium/phospholipid-binding domains of synaptotagmin I [37], a synaptic vesicle membrane protein; and some phospholipases (cytosolic PLA2 [33] and PLCδ1 [38]). On the basis of these homologies, we believe that PEBP may have a similar function and might be a membrane-binding protein, interacting with other proteins and perhaps modulating their catalytic activities. The crystallographic data presented here constitute a solid basis to design genetic experiments that will help to provide new insights into the biological function of PEBP and its potential partners in the cell.

Materials and methods

Crystallization

PEBP was purified from bovine brain as previously described [1]. For the crystallization, PEBP was concentrated to 5 mg/ml in 10 mM Hepes buffer (pH 7.0) and 2 mM dithiothreitol (DTT). Two different crystal forms were obtained using the hanging-drop method with the following crystallization conditions: form I was prepared in 20–25% polyethylene glycol 4000 (PEG 4000), 0.2 M ammonium acetate and 0.1 M acetate buffer (pH 4.6); form II was prepared in 18–25% PEG 8000 and 50 mM KH_2PO_4. Under these conditions, crystals grew as bunches of thin plates after three days (form I) and three weeks (form II). In order to produce thicker single crystals and to accelerate crystal growth, macroseeding in hanging drops was then used routinely. Form I crystals are monoclinic and belong to space group C2 (unit-cell dimensions a = 82.70 Å, b = 33.55 Å, c = 60.07 Å, β = 97.71° with one molecule per asymmetric unit). Form II crystals are orthorhombic and belong to space group $P2_12_12_1$ (unit-cell dimensions a = 44.97 Å, b = 77.30 Å, c = 108.17 Å, with two molecules per asymmetric unit).

As yet, we have not succeeded in cocrystallizing PEBP with its real substrates, GTP or phosphatidylethanolamine, but it was possible to grow crystals of PEBP complexed with the polar head group of phosphatidylethanolamine (phosphorylethanolamine). Crystals of PEBP in complex with phosphorylethanolamine (form III) were obtained in 25–27% PEG 8000 and 100 mM phosphorylethanolamine. These crystals are similar to form II. They are orthorhombic and belong to space group $P2_12_12_1$ (unit-cell dimensions a = 44.20 Å, b = 77.16 Å, c = 107.48 Å, with two molecules per asymmetric unit).

Data collection and phasing

The PEBP crystal structure was solved from the monoclinic crystals using the multiple isomorphous replacement (MIR) method with anomalous scattering. Crystals of two heavy-atom derivatives were characterized at our laboratory with a MAR research imaging plate coupled to a RIGAKU rotating anode with λ = 1.54 Å and at a temperature of 100K. The derivatives were prepared by soaking native crystals under the following conditions: 5 mM $HgCl_2$ (for 48 h) or 5 mM K_2PtCN_4 (for 24 h) in 25% PEG 4000, 0.2 M ammonium acetate, 0.1 M acetate buffer pH 4.6. All the diffraction experiments were carried out at 100K. Before flash freezing, crystals were quickly soaked in a solution consisting of 25% PEG 4000, 15% glycerol, 0.1 M ammonium acetate and 0.1 M acetate buffer, pH 4.6.

Higher resolution experiments were then conducted using synchrotron radiation (Beamline DW32, LURE, Orsay, France) with a MAR research imaging plate system at λ = 0.97 Å and 100K. Further details on data collection are presented in Table 1. The data were integrated and reduced with MOSFLM, version 5.50 [40] and SCALA [41]. Scaling between the different data sets and other calculations were carried out using the CCP4 suite of programs [42]. Mercury sites were identified in isomorphous and anomalous difference Patterson maps for both synchrotron and rotating-anode data; one platinum site was identified in an isomorphous difference Patterson map. Refinement of the heavy-atom sites, the phase calculation and the phase refinement were done with SHARP [43] using both synchrotron and rotating-anode data. The final phase calculation resulted in a figure of merit of 0.65 for acentric reflections (0.68 for centric reflections) for data between 32 and 2.6 Å resolution. The phases were then improved by the density modification method implemented in SOLOMON [44]. The best electron-density map was obtained with data between 32 and 2.9 Å resolution. Model building was carried out from this latter electron-density map using the program O [19] installed on an SGI Indigo II graphic system.

Refinement

The initial crystallographic R factor and free R factor (calculated with 10% of the full data set excluded from the refinement process [45]) for the model that included residues 1–184, and for all the reflections between 8.0 and 1.84 Å resolution, were 52.5% and 51.2%, respectively. These values dropped to 38.4% and 46.5% after one cycle of simulated annealing carried out at 3000K with the program X-PLOR, version 3.851 [46]. Further refinement steps were performed with REFMAC [47] considering all the data between 32 and 1.84 Å resolution. Residue Gly185 and one acetate molecule were easily placed in the resulting electron-density map. Water molecules were identified automatically with ARP [48]. The crystallographic R factor and free R factor decreased to 14.7% and 21.2%, respectively, after the last refinement cycle for all the data between 32 and 1.84 Å resolution.

Table 1

Data collection and phasing.

Data	Native	Mercury	Platinum	Mercury	Form II	Complex
Resolution limit (Å)	1.84	2.5	2.9	2.9	2.4	2.25
Wavelength (Å)	0.97	0.97	1.54	1.54	1.00	1.00
X-ray source	LURE	LURE	Anode	Anode	LURE	LURE
Number of observations	48 585	18 463	9016	10 673	54 972	64 465
Unique reflections	14 517	5918	3620	3517	15 152	16 450
Average redundancy	3.3	3.1	2.5	3.0	3.6	3.9
Data completeness (%)	99.8	93.9	94.9	92.6	97.8	90.8
$<I/\sigma(I)>$	15.8	21.1	25.9	22.3	13.2	12.4
R_{sym}*	0.039	0.033	0.028	0.033	0.056	0.049
Last resolution shell R_{sym}	0.095	0.023	0.047	0.059	0.143	0.122
R_{ano}†	–	0.059	0.029	0.047	–	–
R_{iso}‡	–	0.302	0.073	0.293	–	–
Number of sites	–	2	1	2	–	–
Phasing power (acentric/centric)§	–	3.45/2.15	2.23/1.8	3.88/2.53	–	–
R_{cullis} (acentric/centric)#	–	0.60/0.75	0.77/0.77	0.55/0.75	–	–

*R_{sym} is the measure of the internal consistency of the data, defined as $\Sigma| I_i - <I> | / \Sigma I_i$, where I_i is the intensity of the ith observation and $<I>$ the mean intensity of the reflection. †R_{ano} is the measure of the mean relative anomalous difference between the Bijvoet pairs defined as $\Sigma| <I+> - <I->| / \Sigma| <I+> + <I->|$. ‡$R_{iso}$ is the measure of the mean relative isomorphous difference between the native protein F_P and the derivative F_{PH} data defined as $\Sigma |F_{PH} - F_P| / \Sigma |F_P|$. §The phasing power is defined as $<F_H> / <\varepsilon>$, where $<F_H>$ is the mean heavy-atom contribution and $<\varepsilon>$ the mean lack of closure. #R_{cullis} is defined as $\Sigma | \varepsilon | / \Sigma | F_{PH} - F_P |$. Phasing statistics were given by SHARP output [43]; other statistics were obtained from SCALA [41].

Orthorhombic form and the PEBP–phosphorylethanolamine complex

The final monomeric model was used to locate two PEBP monomers in the orthorhombic crystal form by molecular replacement (AMoRe program [49]). After rigid-body refinement, the structure-factor correlation and the R factor for the best solution were 0.72 and 32.2%, respectively, for data between 15.0 and 4.0 Å resolution. Residual density allowed addition of the backbone atoms of the C-terminal residue (Lys186) and one phosphate ion for each monomer. After one cycle of simulated annealing, carried out at 3000K with X-PLOR version 3.851 [46], further refinement steps with REFMAC [47] and using noncrystallographic symmetry (NCS) restraints (tight restraints in the first steps then loosened restraints were used in the last refinement cycle), led to an R factor and a free R factor of 20.7% and 31.5%, respectively, for all the reflections between 12.5 and 2.4 Å resolution. Water molecules (149) were identified automatically with ARP [48]. The structure of the PEBP–phosphorylethanolamine complex was solved independently by molecular replacement with the monoclinic model and refined using the same procedure as described for the orthorhombic form. The final model includes two PEBP monomers, two phosphorylethanolamine molecules and 163 water molecules. The crystallographic R factor and free R factor are 21.0% and 28.1% for data between 12.5 and 2.25 Å. The data collection statistics are summarized in Table 1.

Accession numbers

The atomic coordinates of the bovine brain PEPB (form I) have been deposited in the Brookhaven PDB with accession code 1a44.

Acknowledgements

We thank Javier Perez at LURE in Orsay and Michel Roth at ESRF Grenoble, for data collection. Special thanks to Patricia Amara, David Pignol and Dominique Housset from IBS, Bertrand Castaing and Hélène Benedetti for help in the preparation of this manuscript. We also thank 'la Ligue départementale contre le Cancer du Loiret' for financial support. BV is a recipient of a Region Centre fellowship.

References

1. Bernier, I. & Jollès, P. (1984). Purification and characterization of a basic 23 kDa cytosolic protein from bovine brain. *Biochem. Biophys. Acta* **790**, 174-181.
2. Bernier, I., Fresca, J.P. & Jollès, P. (1986). Ligand-binding studies with a 23 kDa protein purified from bovine brain cytosol. *Biochem. Biophys. Acta* **871**, 19-23.
3. Bucquoy, S., Jollès, P. & Schoentgen, F. (1994). Relationships between molecular interactions (nucleotides, lipids and proteins) and structural features of the bovine brain 21–23 kDa protein. *Eur. J. Biochem.* **225**, 1203-1210.
4. Bollengier, F. & Mahler, A. (1988). Location of the novel neuropeptide h3 in subsets of tissues from different species. *J. Neurochem.* **50**, 1210-1214.
5. Hori, N., *et al.*, & Matsubara, K. (1994). A human cDNA sequence homologue of bovine phosphatidylethanolamine-binding protein. *Gene* **140**, 293-294.
6. Seddiqi, N., *et al.*, & Schoentgen, F. (1994). Amino sequence of the *homo sapiens* brain 21–23 kDa protein (neuropolypeptide h3) comparison with its counterparts from *Rattus norvegicus* and *Bos taurus* species, and expression of its mRNA in different tissues. *J. Mol. Evol.* **39**, 655-660.
7. Moore, C., Perry, A.C.F., Love, S. & Hall, L. (1996). Sequence analysis and immunolocalisation of phosphatidylethanolamine binding protein (PBP) in human brain tissue. *Mol. Brain Res.* **37**, 74-78.
8. Perry, A.C.F., Hall, L., Bell, A.E. & Jones, R. (1994). Sequence analysis of a mammalian phospholipid-binding protein from testis and epididymis and its distribution between spermatozoa and extracellular secretions. *Biochem. J.* **301**, 235-242.
9. Grandy, D.K., Hanneman, E., Bunzow, J., Shih, M., Machida, C.A., Bidlack, J.M. & Civelli, O. (1990). Purification, cloning and tissue distribution of a 23 kDa rat protein isolated by morphine affinity chromatography. *Mol. Endocrinol.* **4**, 1370-1376.
10. Schoentgen, F., Saccoccio, F., Jollès, J., Bernier, I. & Jollès, P. (1987). Complete amino acid sequence of a basic 21-kDa protein from bovine brain cytosol. *Eur. J. Biochem.* **166**, 333-338.
11. Pikielny, C.W., Hasan, G., Rouyer, F. & Rosbash, M. (1994). Members of a family of *Drosophila* putative odorant-binding proteins are expressed in different subsets of olfactory hairs. *Neuron* **12**, 35-49.

12. Lobos, E., Altmann, M., Mengod, G., Weiss, N., Rudin, W. & Karam, M. (1990). Identification of an *Onchocerca volvulus* cDNA encoding a low molecular weight antigen recognized by onchocerciasis patient sera. *Mol. Biochem. Parasitol.* **39**, 135-146.
13. Gems, D., *et al.*, & Maizels, R.M. (1995). An abundant *trans*-spliced mRNA from *Toxocara canis* infective larvae encodes a 26-kDa protein with homology to phosphatidylethanolamine-binding proteins. *J. Biol. Chem.* **270**, 18517-18522.
14. Robinson, L.C. & Tatchell, K. (1991). TFS1: a suppressor of *CDC25* mutation in *Saccharomyces cerevisiae*. *Mol. Gen. Genet.* **230**, 241-250.
15. Bradley, D., Carpenter, R., Copsey, L., Vincent, C., Rothstein, S. & Coen, E. (1996). Control of inflorescence architecture in *Antirrhinum*. *Nature* **379**, 791-797.
16. Trottein, F. & Cowman, A.F. (1995). The primary structure of a putative phosphatidylethanolamine binding protein from *Plasmodium falciparum*. *Mol. Biochem. Parasitol.* **70**, 235-239.
17. Schoentgen, F., *et al.*, & Mornon, J.P. (1992). Main structural and functional features of the basic cytosolic bovine 21 kDa protein delineated from hydrophobic cluster analysis and molecular modeling. *Protein Eng.* **5**, 295-303.
18. Rossmann, M.G., Moras, D. & Olsen, K.W. (1974). Chemical and biological evolution of a nucleotide-binding protein. *Nature* **250**, 194-199.
19. Jones, T.A., Zou, J.-Y., Cowan, S.W. & Kjeldgaard, M. (1991). Improved methods for building protein models in electron density maps and the location of errors in these models. *Acta Cryst. A* **97**, 110-119.
20. Laskowski, R.A., MacArthur, M.W., Moss, D.S. & Thornton, J.M. (1993). PROCHECK: a program to check the stereochemical quality of protein structures. *J. Appl. Cryst.* **26**, 283-291.
21. Kabsch, W. & Sander, C. (1983). Dictionary of protein secondary structure: pattern recognition of hydrogen-bonded and geometrical features. *Biopolymers* **22**, 2577-2637.
22. Holm, L. & Sander, C. (1993). Protein structure comparison by alignment of distance matrix. *J. Mol. Biol.* **233**, 123-138.
23. Gosser, Y.Q., *et al.*, & Rosen, M.K. (1997). C-terminal binding domain of the Rho GDP-dissociation inhibitor directs N-terminal inhibitory peptide to GTPases. *Nature.* **387**, 814-819.
24. Kleywegt, G.J. & Jones, T.A. (1994). Detection, delineation, measurement and display of cavities in macromolecular structures. *Acta Cryst. D* **50**, 178-185.
25. Nicholls, A., Sharp, K. & Honig, B. (1992). Manual for version 1.04. GRASP: graphical representation and analysis of surface properties.
26. Pai, E.F., Krengel, U., Holmes, K.C., John, J. & Wittinghofer, A. (1989). Structure of the guanine-nucleotide-binding domain of the Ha-ras oncogene product p21 in the triphosphate conformation. *Nature* **341**, 209-214.
27. Sha, B., Phillips, S.E, Bankaitis, V.A. & Luo, M. (1998). Crystal structure of the *Saccharomyces cerevisiae* phosphatidylinositol-transfer protein. *Nature* **391**, 506-510.
28. Flower, J. (1996). The lipocalin family: structure and function. *Biochem. J.* **318**, 1-14.
29. Shin, D.H., Lee, J.Y., Hwang, K.Y., Kim, K.K. & Suh, S.W. (1995). High-resolution structure of a non-specific lipid-transfer protein from maize seedlings. *Structure* **3**,189-199.
30. Stewart, D.E., Sarkar, A. & Wampler, J.E. (1990). Occurrence and role of *cis* peptide bonds in protein structures. *J. Mol. Biol.* **214**, 253-260.
31. Herzberg, O. & Moult, J. (1991). Analysis of the steric strain in the polypeptide backbone of protein molecules. *Proteins* **11**, 223-229.
32. Fisher, A.J., Thompson, T.B., Thoden, J.B., Baldwin, T.O. & Rayment, I. (1996). The 1.5 Å resolution crystal structure of bacterial luciferase in low salt conditions. *J. Biol. Chem.* **271**, 21956-21968.
33. Perisic, O., Fong, S., Lynch, D.E., Bycroft, M. & Williams, R.L. (1998). Crystal structure of a calcium-phospholipid binding domain from cytosolic phospholipase A2. *J. Biol. Chem.* **273**, 1596-1604.
34. Bradley, D., Ratcliffe, O., Vincent, C., Carpenter, R. & Coen, E. (1997). Inflorescence commitment and architecture in *Arabidopsis*. *Science* **275**, 80-83.
35. Wlodawer, A., Bott, R. & Sjolin, L. (1982). The refined crystal structure of ribonuclease A at 2.0 Å resolution. *J. Biol. Chem.* **257**, 1352-1332.
36. Karplus, P.A., Daniels, M.J. & Herriott, J.R. (1991). Atomic structure of ferredoxin-NADP$^+$ reductase: prototype for a structurally novel flavoenzyme. *Science* **251**, 60-66.
37. Sutton, R.B., Davietov, B.A., Berghuis, A.M., Südhof, T.C. & Sprang, S. (1995). Structure of the first C2 domain of synaptotagmin I: a novel Ca^{2+}/phospholipid fold. *Cell* **80**, 929-938.
38. Essen, L.O., Perisic, O., Cheung, R., Katan, M. & Williams, R.L. (1996). Crystal structure of a mammalian phosphoinoside-specific phospholipase C delta. *Nature* **380**, 595-602.
39. Bruun, A.W., Svendsen, I., Sorensen, S.O., Kielland-Brandt, M.C. & Winther, J.C. (1998). A high affinity-inhibitor of yeast carboxypeptidase Y is encoded by TFS1 and shows homology to a family of lipid binding proteins. *Biochemistry* **37**, 3351-3357.
40. Leslie, A.G.W. (1990). *Crystallography Computing*. Oxford University Press, UK.
41. Evans P.R. (1993). Data reduction. In *Proceedings of the CCP4 Study Weekend on Data Collection and Processing*. pp. 114-122, SERC Laboratory, Daresbury, Warrington, UK.
42. Collaborative Computational Project No. 4. (1994). The CCP4 suite; programs for protein crystallography. *Acta Cryst. D* **50**, 760-763.
43. La Fortelle, E. & Bricogne, G. (1997). Maximum-likelihood parameter refinement program for MIR and MAD phasing. *Methods Enzymol.* **276**, 472-494.
44. Abrahams, P.J. & Leslie, A.G.W. (1996). Methods used in the structure determination of bovine mitochondrial F_1 ATPase. *Acta Cryst. D* **52**, 30-42.
45. Brünger, A.T. (1992). The free R value: a novel statistical quantity for assessing the accuracy of crystal structures. *Nature* **355**, 472-474.
46. Brünger, A.T. (1992). *X-PLOR Version 3.1: a System for X-ray Crystallography and NMR.* Yale University Press, New Haven, USA.
47. Murshudov, G., Vagin, A.A. & Dodson, E.J. (1997). Refinement of molecular structures by the maximum-likelihood method. *Acta Cryst. D* **53**, 240-255.
48. Lamzin, V.S. & Wilson, K.S. (1993). Automated refinement of protein models. *Acta Cryst. D* **49**,129-147.
49. Navaza, J. (1993). On the computation of the fast rotation function. *Acta Cryst. D* **49**, 588-591.
50. Carson, M. (1997). Ribbons. *Methods Enzymol.* **277**, 493-505.
51. Kraulis, P.J. (1991). MOLSCRIPT: a program to produce both detailed and schematic plots of protein structures. *J. Appl. Cryst.* **24**, 946-950.
52. Read, J.R. (1986). Improved Fourier coefficients for maps using phases from partial structures with errors. *Acta Cryst. A* **42**, 140-149.
53. Johnston, M., *et al.*, & Hoheisel, J.D. (1997). The nucleotide sequence of *Saccharomyces cerevisiae* chromosome XII. *Nature* **387**, 87-90.